Mechanical Systems and Signal Processing 145 (2020) 106959

Contents lists available at ScienceDirect

Mechanical Systems and Signal Processing

journal homepage: www.elsevier.com/locate/ymssp

Experimental study on active seismic isolation using interferometric inertial sensors

G. Zhao [a,*], B. Ding [a,*], J. Watchi [a], A. Deraemaeker [b], C. Collette [a,c,*]

[a] Université Libre de Bruxelles, Precision Mechatronics Laboratory, Beams Department, F.D. Roosevelt Av 50, 1050 Brussels, Belgium
[b] Université Libre de Bruxelles, BATir Department, F.D. Roosevelt Av 50, 1050 Brussels, Belgium
[c] University of Liege, Department of Aerospace and Mechanical Engineering, Allée de la Découverte 9, 4000 Liege, Belgium

ARTICLE INFO

Article history:
Received 25 October 2019
Received in revised form 23 April 2020
Accepted 28 April 2020
Available online 7 May 2020

Keywords:
Inertial sensor
Interferometric
Tilt-vertical coupling
Active seismic vibration isolation

ABSTRACT

The goal of this study is to demonstrate the capability to actively isolate a platform from seismic vibrations using an interferometric inertial sensor. To this purpose, a homemade high-resolution interferometric uni-axial inertial sensor (in the vertical direction) is developed and then integrated to a single-degree-of-freedom (SDOF) seismic isolation system. A theoretical study is firstly performed in order to better understand the dynamics of the system. It is found that the sensor suffers from a tilt-vertical coupling due to the influence of the gravity force if the sensor is not perfectly aligned. By taking this tilt coupling into account, a dedicated controller is designed, seeking a large vibration isolation in the frequency band of interest. Experiments are then conducted for validating the theoretical analysis and examining the vibration isolation performance. It shows a reduction of the transmitted motion of up to 60 dB in a frequency range from 0.1 Hz to 10 Hz.

1. Introduction

Isolation from seismic vibrations is a major concern in many fields, for example, to ensure the safety of ground-based infrastructures [1–3], to allow conducting precise experiments [4–6], or to manufacture small components [7]. Soft supports such as pneumatic elements [8,9] or mechanical springs [9,10] whose effective stiffness can be reduced thanks to negative stiffness mechanisms [11–14], are often used for seismic isolation applications. These supports are referred to as passive isolation systems which are only effective above the suspension resonance while seismic vibrations fully transmit through the suspensions below the resonance. Therefore, for applications requiring a good isolation at low frequency (say, below 1 Hz), these passive isolators often fail to mitigate the transmission of seismic motion, due to the difficulty of building compact isolators with a fundamental frequency smaller than 0.5 Hz. Consequently, the isolation has to be obtained using active control. For example, active seismic isolation systems (ASIS) are particularly required for large instruments dedicated to experimental physics, like synchrotrons, particle colliders [15] and gravitational wave detectors [16,17]. In addition, active isolation systems have also been developed for the stabilization of atomic gravimeters [18,19]. In order to develop an appropriate ASIS, a couple of considerations such as (1) structural resonances, (2) sensor noise and (3) couplings need to be addressed [20].

For the first concern, the mechanical structure of ASIS should be carefully designed such that its flexible mode resonances are well separated from the frequency band of interest. If this is not the case, see for example in Ref. [17,21], sophisticated

* Corresponding authors.
E-mail address: guoying.zhao@ulb.ac.be (G. Zhao).

https://doi.org/10.1016/j.ymssp.2020.106959
0888-3270/

controllers would be needed to achieve an acceptable isolation performance. This however often exhibits poor robustness. As the design of ASIS is more case specific, it is not studied in this paper.

For the second issue i.e. sensor noise, inertial sensors are typically used for implementing ASIS which measure the relative motion between the sensor reference mass and the platform. By nulling the output of the sensor, the platform is forced to track the motion of the reference mass of the sensor thereby isolated as well from ground seismic vibrations. If perfect controllers can be realised, the performance of ASIS would be mainly limited by the performance of the inertial sensors i.e. the residual motion of the platform would eventually converge to the noise floor of the sensors [17,22,23]. Although first choice commercially available inertial sensors can reach a sufficient resolution to measure natural ground motion in a wide frequency band, their resolution and the dynamic range remain limited at low frequency. The limitation can be caused for example by thermal noise of the mechanics [24], electronics noise of signal amplifiers [25], environmental variations such as changes of temperature, pressure and magnetic field etc. [26], noise of control systems for force-feedback sensors [27] and non-linear couplings [28]. Moreover, the sensors realised with electromagnetic transducers such as geophone (Mark L4C), seismometers (Güralp CMG–6T and *STS-1V*) are known to be sensitive to the surrounding magnetic field. This would prevent them from being integrated into active isolation systems [17]. Recently, optical, non-feedback inertial sensors have been investigated [29–31]. Optical displacement transducers were reported to exhibit good performances i.e. high resolution, large dynamic range and low sensitivity to environmental noise. The elimination of the force-feedback technique would allow for a mitigation of the control system noise. However, the reported optical, non-feedback inertial sensors are mainly laboratory made instruments which are not commercially available nor yet examined for the active seismic isolation applications. In this paper, a homemade interferometric inertial sensor (INIS) is presented despite a large margin of performance improvement is foreseen. The main focus of this paper is to investigate the feasibility and effectiveness of using the INIS to actively isolate a payload from vertical seismic vibrations in a low frequency range between 0.1 Hz and 10 Hz.

Another barrier for extending the isolation performance at low frequency is the horizontal-tilt coupling [32,33] which arises when the inertial feedback technique is applied in the horizontal direction. This is because horizontal inertial sensors cannot distinguish the contributions from actual horizontal motions and that from tilt motions. In this paper, it is found that vertical inertial sensors are also prone to the tilt coupling. Unlike the horizontal-tilt coupling which exists unconditionally, the vertical tilt coupling only occurs when vertical inertial sensors are not perfectly aligned with gravity. This is considered as another contribution of this study.

The rest of the paper continues as follows. Section 2 presents the design of the INIS and its dynamic response to translational and rotational excitations is described in Section 3. Section 4 presents the SDOF test bench, along with experimental results of active seismic isolation using the INIS. Finally, Section 5 draws the conclusions.

2. Development of interferometric inertial sensor

The INIS is shown in Fig. 1 (a) and its sketch is depicted in Fig. 1 (b). The INIS is mainly composed of two subsystems: (i) a homemade interferometric readout, (ii) a mechanical harmonic oscillator modified from the structure of the *STS-1 V* seismometer [27]. The idea behind is to replace the original electromagnetic motion transducers and the force feedback systems of the *STS-1 V* seismometer with a homemade interferometric readout to measure the motion of the reference mass. For the interferometric readout, a single polarised beam from a frequency stabilised fibre laser source with a wavelength of 1550 nm (*Koheras Adjustik X15*) is used. The laser beam transmits sequentially through a collimator (F280APC-1550), a polarising beam splitter (PBS1, *PBS204*), a quarter wave plate (*WPQ10E-1550*), a non-polarising beam splitter (BS, *BS018*), a half wave plate (*WPH10E-1550*), another polarising beam splitter (PBS2) and finally reaches to the corner cube 1 and 2 (*PS974M-C*) which are mounted on the sensor frame and the reference mass, respectively. The beams returned from the two corner cubes are then recombined at PBS2 and co-propagate without interfering. On the way back, the beams interfere at the polarizer and the PBS1. The corresponding interference pattern is measured by two photodiodes: PD1 and PD2 (*PD50B-EC*), respectively. Between BS and PBS1, the quarter wave plate is employed which adds an additional 90° phase shift to the intensity fluctuation measured by PD2 compared to that of PD1. Compared to common Michelson interferometers, the implemented interferometer helps improve the dynamic range of the readout. More details of the optical readout and the corresponding signal processing method for dealing with the quadrature signals can be found in Ref. [34]. For the subsystem (ii), it consists of a reference mass which is suspended from the frame with a cross hinge and a leaf spring. Finally, the two subsystems are placed inside a vacuum chamber in order to avoid the influence from the air fluctuation. The dimensions of the kernel of the INIS and the chamber are finalized as 170 mm*110 mm*200 mm (length*width*height) and 336 mm*356 mm (diameter*height), respectively.

Similar to other types of inertial sensors, a low resonance frequency of the mechanical oscillator is preferred as it allows a good sensitivity at low frequencies. For the employed structure which is modified from the *STS-1 V* seismometer, a resonance frequency of 0.3 Hz is realised.

The performance of the developed sensor is preliminarily assessed by comparing with a benchmark sensor *Guralp 6 T* sensor[1]. The *Guralp* and the developed INIS are placed on the ground next to each other to measure the same seismic motion. Fig. 2 plots the transfer function and the coherence between the interferometric sensor (INIS) and the *Guralp*. As the sensitivity of the

[1] http://www.guralp.com/documents/DAS-T60-0001.pdf.

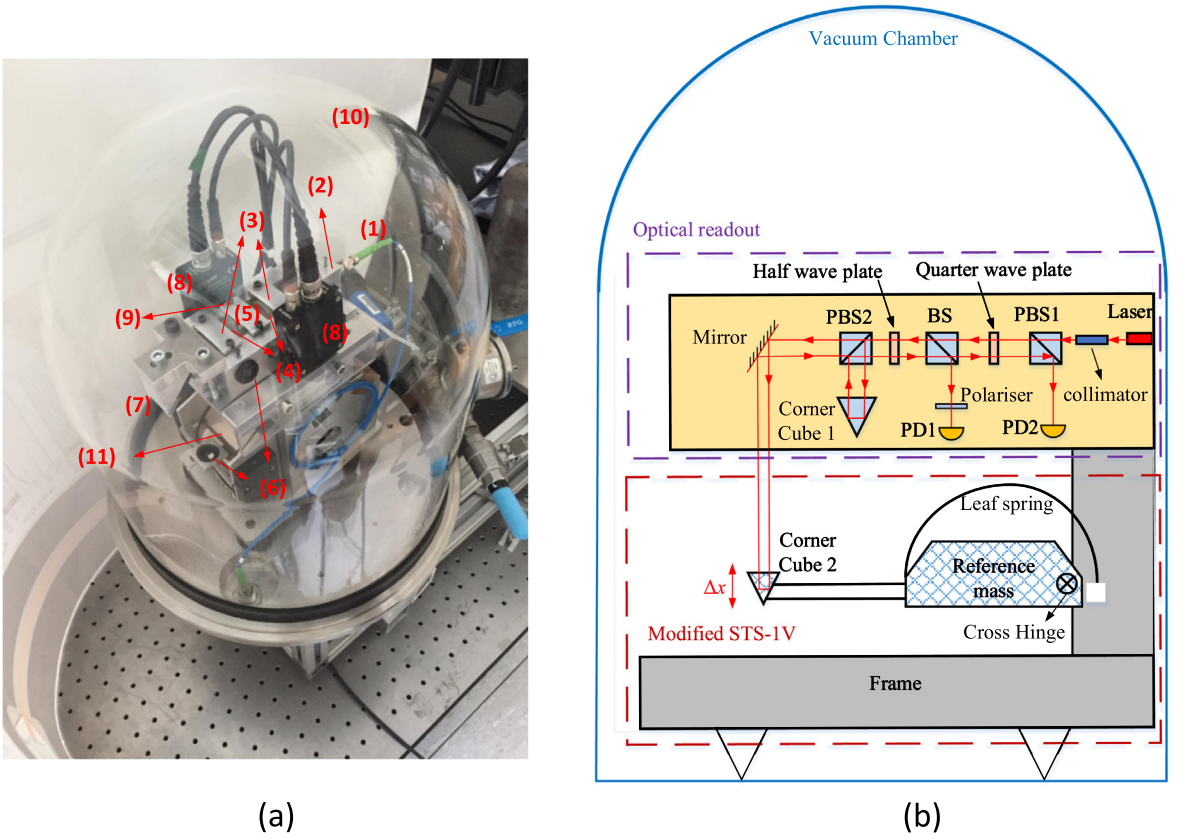

Fig. 1. (a) Picture of the interferometric inertial sensor: (1) fibre laser, (2) collimator, (3) polarising beam splitter, (4) wave plates, (5) beam splitter, (6) corner cube (7) mirror, (8) photodiode, (9) polariser, (10) vacuum chamber and (11) modified *STS-1V* mechanism; (b) its simplified sketch.

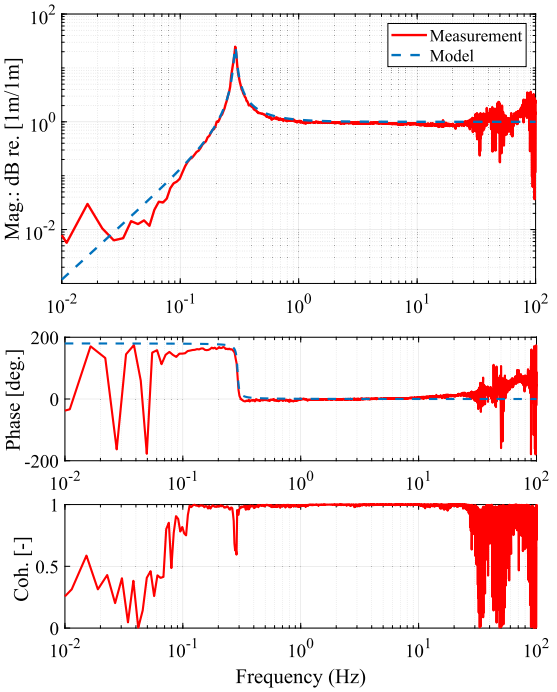

Fig. 2. The frequency response of the transfer function between the INIS and the *Guralp* and its coherence under local seismic vibration excitation.

Guralp has a flat frequency response over the range of 0.1 Hz − 100 Hz, it alternatively means that the sensitivity of the INIS can be characterised by a linear SDOF model as can be seen from the magnitude and the phase plot. This model with the following parameters kg - mass weight, $k = 2.01$ N/m – suspension stiffness and $d = 0.044$ N/(m/s) – damping coefficient corresponding to damping ratio of 2% is developed and reported in the same figure (dashed line) for comparison. As depicted in the coherence plot, this model only validates between 0.1 Hz and 30 Hz. While above 30 Hz, the spurious resonances of the INIS start to present which cannot be represented by the developed SDOF model. On the other hand, below 0.1 Hz, the sensitivity of the INIS decreases whereas incoherent noises are recorded causing the drop of the coherence between the two sensors. Nevertheless, it is shown that the developed INIS is capable of capturing the ground motion in the frequency range between 0.1 Hz and 30 Hz.

3. Interferometric inertial sensor mounted on the platform

In the previous section, where the sensor is considered as a uni-axial system, the sensor is only sensitive to the vertical disturbances. However, in practice, the sensor is also sensitive to rotational excitations. Therefore, the response of the sensor to both excitations is studied in the following sections.

3.1. Response to vertical motion

A representative model of the INIS is shown in Fig. 3, where the locations of the hinge, the centre of mass and the optical transducer are denoted as o_1, o_2 and o_3, respectively. The reference mass is suspended from the frame with a rotational spring and dash-pot with the coefficients of k_τ and d_τ. The distance between o_1 and o_2, and that between o_1 and o_3 are denoted as L and R, respectively. The reference mass is assumed to be initially inclined from the horizontal axis with an angle α_0 and its instant angular position is represented by α. Now, the developed model allows representing an initial inclination of the reference mass, and thus taking the gravity force into consideration.

Applying Newton's second law of rotation about the hinge o_1 when the system is excited by a pure translational motion denoted by w, the governing equations of the INIS under translational excitations can be derived as follows:

$$I\ddot{\alpha} = -k_\tau\alpha - d_\tau\dot{\alpha} + mgL\ \cos\ \alpha + mL\ddot{w}\ \cos\ \alpha \tag{1}$$

$$x = -R(\alpha - \alpha_0) \tag{2}$$

where m is the reference mass, I is the moment of the inertia with respect to the hinge o_1 and x represents the relative displacement between the instant location and its equilibrium, calculated assuming the system in small oscillations regime.

Substituting Eq. (2) into Eq. (1), yields:

$$I\ddot{x} + k_\tau x - k_\tau R\alpha_0 + d_\tau\dot{x} = -mRL\left(\ddot{w}\ \cos\ \alpha_0 + \ddot{w}\frac{x}{R}\ \sin\ \alpha_0 + g\ \cos\ \alpha_0 + g\frac{x}{R}\sin\alpha_0\right) \tag{3}$$

where an approximation $x/R \approx \sin\ (x/R)$ is applied.

At the equilibrium, $k_\tau\alpha_0 = mgL\cos\alpha_0$, Eq. (3) then turns into:

$$I\ddot{x} + k'_\tau x + d_\tau\dot{x} = -mRL\ddot{w}\cos\alpha_0 \tag{4}$$

where $k'_\tau = k_\tau + mgL\sin\alpha_0$ and the coefficient $\frac{x}{R}\sin\alpha_0$ for $\ddot{w}$ is neglected considering both x and α_0 are small quantities.

Eq. (4) indicates that the suspension of the sensor is stiffened due to the sine coupling of the gravity and the vertical ground motion is less sensed because of the cosine coupling. The horizontal tilt coupling is not considered here as the initial inclination α_0 is assumed to be small.

3.2. Response to rotational motion

Fig. 4 shows the model of the scenario when the sensor is only subjected to a rotational excitation Ω. All the other notations remain the same as that in the previous section.

In this case, the governing equation is written as:

$$I\ddot{\alpha} = -k_\tau\alpha - d_\tau\dot{\alpha} + I\ddot{\Omega} + mgL\cos\left(\Omega - \alpha\right) \tag{5}$$

Substituting Eq. (2) into Eq. (5), yields:

$$I\frac{\ddot{x}}{R} + k_\tau\left(\frac{x}{R} - \alpha_0\right) + d_\tau\left(\frac{\dot{x}}{R}\right) = -I\ddot{\Omega} - mgL\cos\left(\Omega + \frac{x}{R} - \alpha_0\right) \tag{6}$$

Expanding $\cos\left(\Omega + \frac{x}{R} - \alpha_0\right)$, gives:

$$\cos\left(\Omega + \frac{x}{R} - \alpha_0\right) = \cos\Omega\left(\cos\frac{x}{R}\cos\alpha_0 + \sin\frac{x}{R}\sin\alpha_0\right) - \sin\Omega\sin\left(\frac{x}{R} - \alpha_0\right) \tag{7}$$

Considering that Ω, x and α_0 are small quantities, Eq. (7) is simplified to:

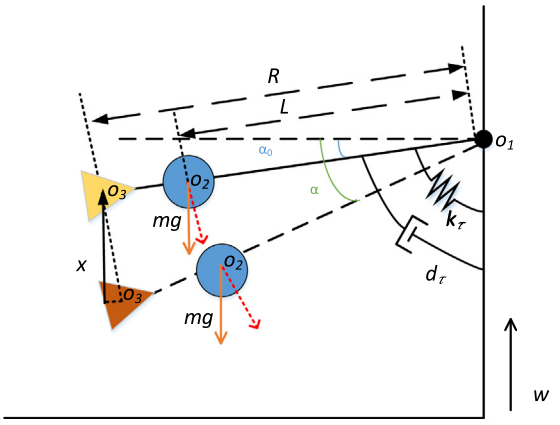

Fig. 3. The representative model of the INIS under only vertical excitations.

$$\cos\left(\Omega+\frac{x}{R}-\alpha_0\right)=\cos\alpha_0+\frac{x}{R}\sin\alpha_0+\Omega\sin\alpha_0 \tag{8}$$

where an approximation $x/R\approx\sin(x/R)$ is applied.

Substituting Eq. (8) into Eq. (6), yields,

$$I\frac{\ddot{x}}{R}+k_\tau\left(\frac{x}{R}-\alpha_0\right)+d_\tau\left(\frac{\dot{x}}{R}\right)=-I\ddot{\Omega}-mgL\left(\cos\alpha_0+\frac{x}{R}\sin\alpha_0+\Omega\sin\alpha_0\right) \tag{9}$$

At equilibrium, as the same for the translational excitation case, Eq. (9) then turns into:

$$I\ddot{x}+k'_\tau x+d_\tau\dot{x}=-RI\ddot{\Omega}-mgRL\Omega\sin\alpha_0 \tag{10}$$

According to Eq. (10), there is one frequency at which the right hand terms cancel out leading to a complete loss of the sensitivity transfer function at this particular frequency, termed zero of the sensor sensitivity. It is noted that the location of this frequency is proportional to the initial inclination and this phenomenon only occurs when the sensor is subject to rotational motions. It should be also noticed that there are two real zeros when the initial inclination α_0 is negative. One of them is located on the right half plane. In such a scenario, the closed-loop system would become unstable if a high loop gain is applied.

When both disturbances are present, the sensor dynamics can be derived by combining the inputs from Eqs. (4) and (10):

$$I\ddot{x}+k'_\tau x+d_\tau\dot{x}=-mRL\ddot{w}\cos\alpha_0-RI\ddot{\Omega}-mgRL\Omega\sin\alpha_0 \tag{11}$$

4. Experimental validation

A representative set-up for a SDOF system, as shown in Fig. 5 (a), is constructed in order to examine the active vibration isolation performance using the customised INIS. It consists of a rigid frame, mounted on a knife hinge, and restrained by a

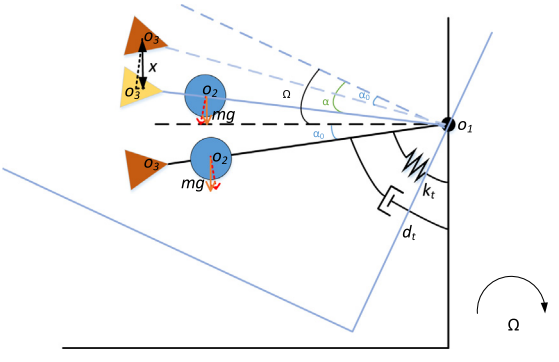

Fig. 4. The representative model of the INIS under only rotational excitations.

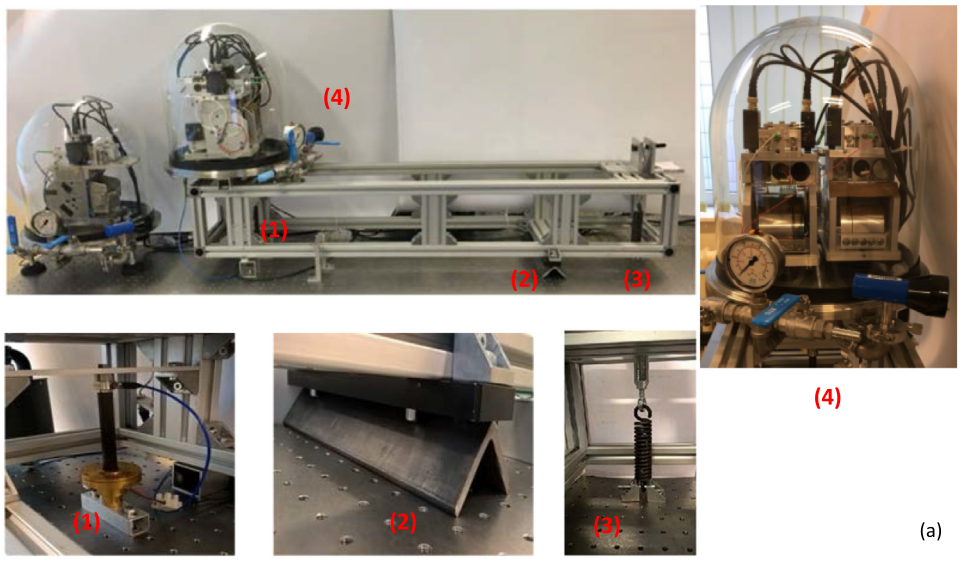

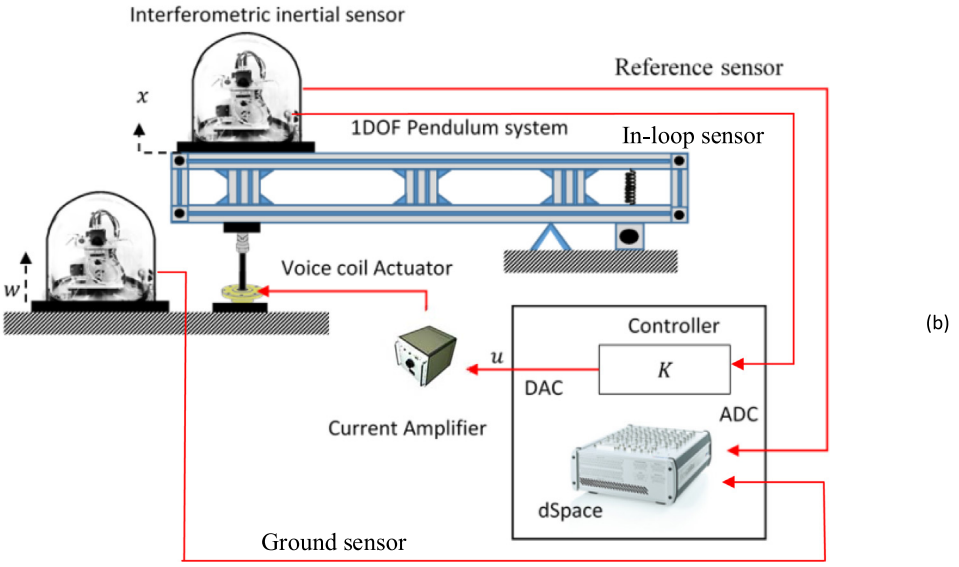

Fig. 5. (a) Picture of the experimental set-up and (b) its simplified sketch: (1) voice coil actuator, (2) knife hinge, (3) metallic spring and (4) side view of the modified INIS.

metallic spring (on the right hand side of the setup). The free end of the frame is attached with a voice coil actuator (home-made), and the vertical motion is measured by the INIS.

Fig. 6 (a) depicts the sketch of the SDOF pendulum system. Two new notations are introduced: R_0, the distance between the hinge o_1 and the knife hinge o_4, and β, the initial orientation of o_1-o_4 with respect to the horizontal axis. All the other ones remain the same as shown previously. In order to simplify the analysis, a simplified sketch as shown in Fig. 6(b) is used where Ω_0 represents the rotational motion of the frame with respect to the knife hinge o_4. Ω_0 is essentially determined by the ground motion and the dynamic interactions between the sensor and the frame. In the following, Ω_0 is directly imposed as a disturbance source and the corresponding interactions are neglected.

Considering now the hinge point of the sensor o_1, it actually undergoes a rotational disturbance Ω_0 and a translational disturbance w_0 (in the vertical direction) which is induced by the rotation Ω_0. w_0 can be approximated as:

$$w_0 = R_0(\sin(\beta + \Omega_0) - \sin\beta) \approx R_0\Omega_0 \cos\beta \tag{12}$$

Substituting w_0 as given in Eq. (12) and Ω_0 into Eq. (11), yields:

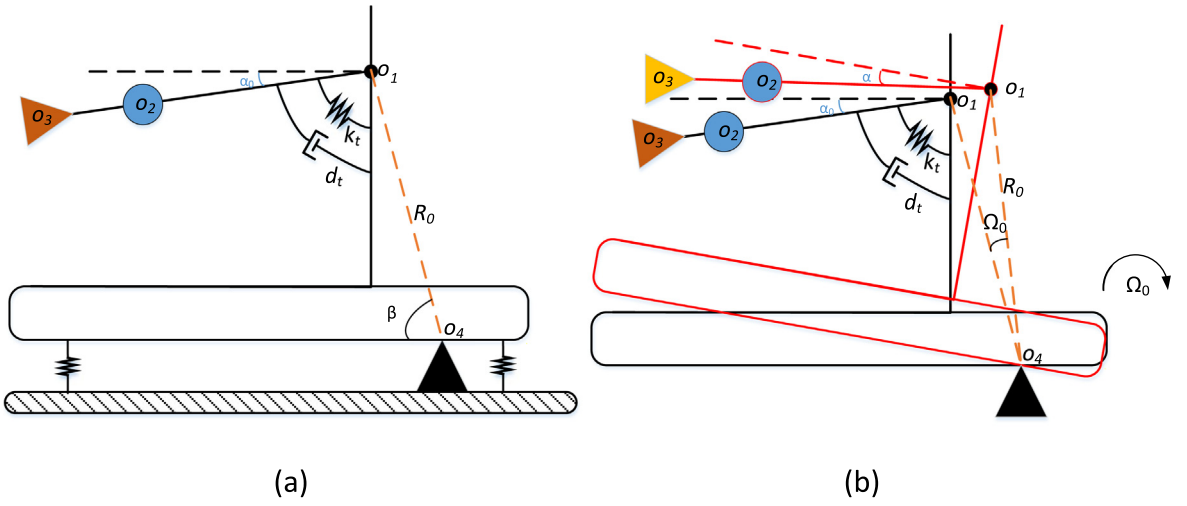

Fig. 6. The geometrical sketch of the INIS mounted on the SDOF set-up under (a) no excitations and (b) translational and rotational excitations.

$$I\ddot{x} + k'_\tau x + d_\tau \dot{x} = -(mLRR_0 \cos\beta \cos\alpha_0 + RI)\ddot{\Omega}_0 - (mgRL \sin\alpha_0)\Omega_0 \tag{13}$$

As shown in Eq. (13), there is one pair of conjugate zeros in the transfer function between the sensor output x and the excitation Ω_0, and its location is initial inclination angle and geometrical parameters dependent. For example, an increase of the inclination angle α_0 would result in an increase of the frequency location of the zero.

In the following, experimental results will be presented focusing on: (1) the validation of the dynamic analysis of the sensor and (2) the investigation of the potential using the INIS for low frequency active isolation applications. Prior to describing the results obtained, some system parameters are defined. During the experimental study a *dSpace MicroLabBox* system has been used both for data acquisition and for control purposes. The whole control scheme is implemented in the *MATLAB Simulink* environment and then downloaded to the processor unit of the *MicroLabBox* system. The feedback control scheme runs at 10 kHz frequency, but the measured data are recorded at frequency of 1 kHz reducing the memory usage for data storage.

The layout of the sensor configuration is shown in Fig. 5(b), where one INIS is placed on the ground to measure the ground motion, and another two INISs are mounted side by side in the same vacuum chamber which sits on the free end of the SDOF system recording the frame motion. One of the two redundant sensors on top of the frame is chosen as the error signal (termed in-loop sensor) to drive the voice coil actuator through a current amplifier (*ADD-45N*) and the other one is used as a reference sensor (termed reference sensor) to objectively measure the frame motion.

The control plant from the actuator to the in-loop sensor is identified first. This is done by injecting a white noise into the actuator and simultaneously recording this driving signal and the output of the in-loop sensor. The frequency response of the control plant is shown in Fig. 7 (blue curve). The curve mainly exhibits two peaks. The first one at 0.3 Hz corresponds to the sensor resonance, while the second one at 2 Hz corresponds to the SDOF pendulum resonance. The lack of coherence below 0.1 Hz is caused by the low signal to noise ratio. During this experiment, the excitation level of the actuator is limited to avoid saturations of the sensors at the resonances. In order to improve the quality of the measurement of the control plant at low frequency, sinusoidal excitations are alternatively used. Here, a number of frequency points are selected between 10 mHz and 90 mHz to perform the identification measurement. The resultant frequency response is superimposed in Fig. 7. It can be seen that there is one zero identified at 0.0625 Hz. This indicates that the sensor is not perfectly aligned, but with a positive initial inclination. Fig. 7 further shows the model of the control plant denoted as G, which is obtained by fitting the experimental data:

$$G = \frac{0.022s(s^2 + 0.0031s + 0.15)(s^2 + 3.13s + 12510)}{(s + 0.6)(s^2 + 0.09s + 3.67)(s^2 + 0.19s + 138.8)(s^2 + 3.39s + 11952)} \tag{14}$$

In order to further investigate the origin of the zero, the stepped sine excitation experiment is repeated when the static inclination of the frame of the SDOF pendulum system is tuned to 0.09° and 0.12°, respectively. This can be done by adjusting the set screw on the restoring spring and the inclination angle is measured by a digital protractor (*Pro3600*) with a resolution of 0.01°. It should be noted that the inclination change of the frame is not precisely equal to that of the INIS, but the same tendency holds i.e. the inclination of the INIS also increases with an increase of the frame inclination. Fig. 8 shows the frequency response of the control plant in the vicinity of the zeros. As predicted by Eq. (13) the location of the zero indeed increases with an increase of the initial inclination.

It has to be mentioned that the initial phase of 90° at low frequency is due to the use of a lead compensator (a derivative filter), which is introduced in order to remove the static component from the post-processing of the sensor signals.

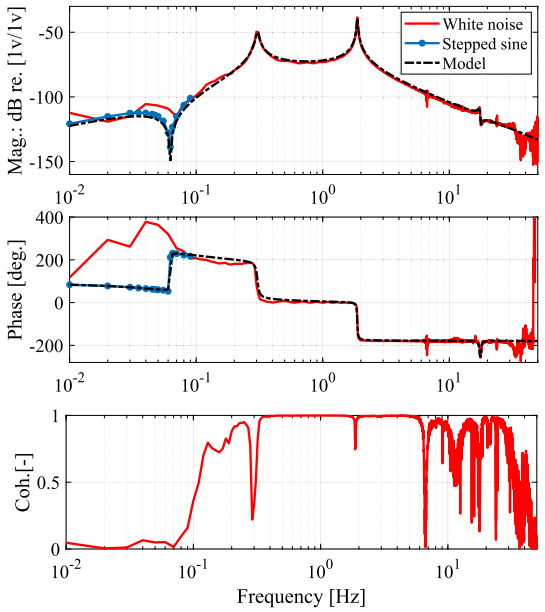

Fig. 7. Measurement and modelling of the control plant between the actuator and the in-loop sensor.

With the identified control plant, a digital controller C is proposed aiming to achieve a high open loop gain in a frequency range from 10 mHz to 10 Hz. This controller C is given as:

$$C = \frac{2.2 \times 10^6 (s+2.3)^2 (s+3.1)(s+7.4)(s+90.5)(s^2+3.39s+11952)}{(s+0.23)(s+0.32)(s+0.42)(s+53.5)(s+425.5)(s^2+3.13s+12510)} \tag{15}$$

The double real zeros located at $s = -2.3$ and the two real poles $s = -0.23, \quad s = -0.32$ are deployed such that they counteract the first pair of complex zeros and poles of the control plant in the phasewise sense. The real zero $s = -3.1$ and the real pole $s = -0.42$ are paired, which introduces certain phase lags, in order to have sufficient phase margins in the low frequency range. Two lead filters with zeros at $s = -7.4$, $s = -90.5$ and poles $s = -53.5$, $s = -425.5$ are used to introduce some phase margins in the high frequency range. The complex zeros and poles in the controller C are introduced based on the plant inversion such that they neutralise the effects of the corresponding complex poles and zeros of the control plant.

Fig. 9 plots the frequency response of the control plant G, the open loop gain defined as GC and the closed loop sensitivity defined as $1/(1+GC)$. It is seen that a reduction up to 60 dB can be achieved in terms of the frame vibrations between 10 mHz and 10 Hz. The loss of the control effectiveness around this zero is because the sensor is not able to measure the frame motion so that there is no control observability at this frequency. Close to 10 Hz, the control performance gradually degrades as the frequency approaches the unit gain frequency (approximately 20 Hz).

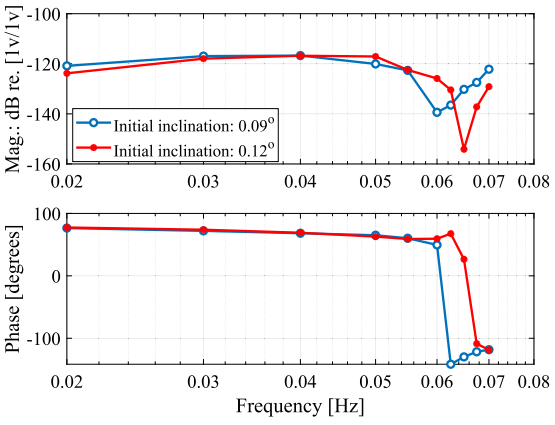

Fig. 8. The frequency response of the transfer function between the excitation and the in-loop sensor when the initial inclination of the frame is set to 0.09° and 0.12°.

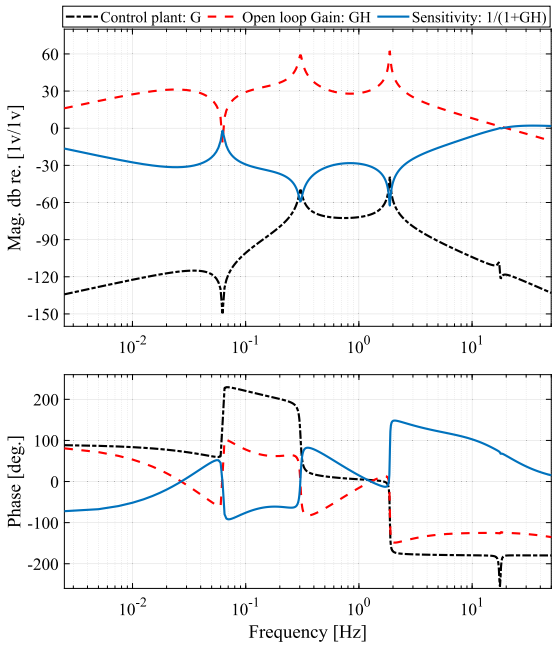

Fig. 9. The frequency response of the control plant, the open loop gain and the closed loop sensitivity.

The performance of the proposed controller is also experimentally examined. The local seismic vibration is considered as the excitation source and the control effort aims to isolate the transmission of the ground vibration to the primary system as shown in Fig. 5. Fig. 10 compares the Amplitude Spectral Densities (ASD) of the in-loop sensor and the reference sensor when the controller is turned off and on, as well as that of another INIS placed on the ground i.e. the optical table and the noise floor of the INIS. Note that the outputs of the INISs are normalized according to the mechanical sensitivities, as identified in Fig. 2. The noise floor is obtained by running a huddle test on the signals measured by the in-loop sensor and the reference sensor when the controller is switched off. The idea behind is to subtract the incoherent signal from the two sensors, which is then assumed to be noise floor of the sensor. The corresponding coherence between the in-loop sensor and the reference sensor for the two cases is depicted in Fig. 11. The duration of the measurement is set to 2000 s.

When the controller is inactive, the in-loop sensor and the reference sensor are supposed to measure the same quantity i.e. the motion of the frame. This is the case in the frequency range between 0.1 Hz and 4 Hz, where the ASD of the in-loop sensor coincides well with that of the reference sensor and the coherence is almost equal to unity except around the resonances of the sensors. It is also seen that the ASDs of the two sensors are well distanced from the noise floor, where the dynamic range of the INIS can be greater than three order of magnitude. The noise floor exhibits two peaks around 0.3 Hz. This is because the two sensors do not have the same resonance frequency so that the frame motion is detected incoherently by the two sensors around their resonance frequencies leading to the unsuccessful subtraction of the noise floor in this range. Below 0.1 Hz, the ASDs of the two sensors almost overlap with the noise floor and the coherence decreases with a decrease of frequency. This is caused by the predominance of the sensor noise over the signal proportional to the frame motion. Above 4 Hz, the ASDs of the two sensor cannot be well distinguished from the noise floor either and a poor coherence is observed accordingly. This may be due to the less pronounced frame motion because of the passive isolation, nonlinear coupling of the INIS and flexible dynamics of the frame and the INIS.

When the controller is active, it is seen that the experimental result shown by the in-loop sensor agrees very well with the theoretical prediction, where a reduction of the frame motion up to 60 dB is obtained. The simulation result is obtained by taking the product of the ASD of the in-loop sensor when the controller is inactive and the closed loop sensitivity $1/(1+GC)$ as shown in Fig. 9. More interestingly, it is clearly shown by the in-loop sensor and the reference sensor that the frame motion is reduced by 30 dB at the seismic resonance around 0.15 Hz. However, the in-loop sensor does not exhibit the same trend as the reference sensor in three places: from 10 mHz to 100 mHz (except around 60 mHz), around 0.3 Hz and above 3 Hz. For the first range and the third range, this is because the sensor noise dominates that sensor output whereas the actuator is driven to force the frame to follow the noise of the in-loop sensor instead of eliminating the motion transmission. Around 0.3 Hz, the extra reductions are not observed by the reference sensor. This is due to fact that its resonance frequency is slightly different to that of the in-loop sensor. In other words, it means that the sensitivity of the reference sensor is not as good as that of the in-loop sensor at 0.3 Hz thereby the noise of the reference sensor dominates its output when the controller is activated and the actual motion of the frame is not precisely measured by the reference sensor around this frequency. Around the frame resonance i.e. 2 Hz, both the signals measured by the in-loop sensor and the reference sensor

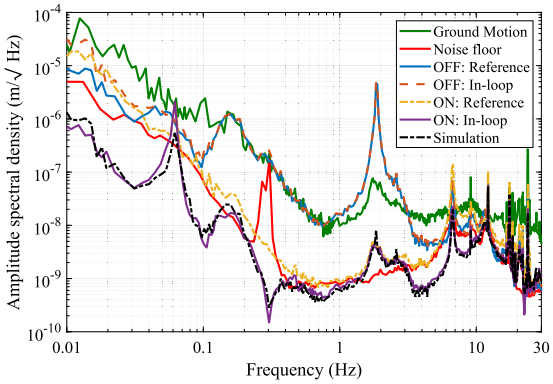

Fig. 10. Comparison of the ASDs of the reference sensor, in-loop sensor when control is on and off, and that of the ground sensor and the noise floor.

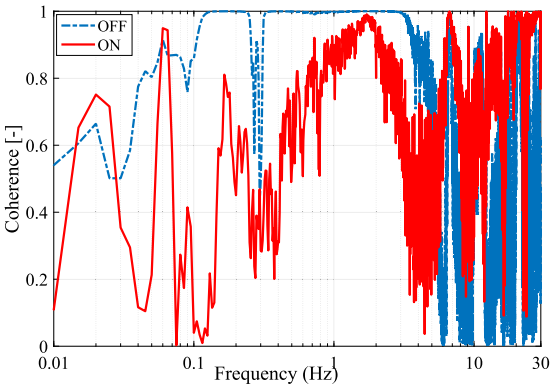

Fig. 11. Comparison of the coherence between the reference sensor and the in-loop sensor when control is on and off.

are slightly above the noise floor and the corresponding coherence is also relatively high. This indicates that the controller is not effective enough to suppress the frame motion, so that the in-loop sensor and the reference sensor are still correlated around this frequency measuring the common frame motion. Due to the presence of the flexible modes of the frame, it is difficult to further push the isolation performance without compromising the stability of the system. Alternatively, a narrow band feedforward controller could be introduced as a supplement to the feedback controller [35], it is however not investigated in the paper.

5. Conclusion

This paper has presented an experimental demonstration of low frequency seismic isolation system using a homemade interferometric inertial sensor. The first part of the paper has been dedicated to the study of the sensor dynamics, in response to vertical and rotational excitations. It is found that the dynamic behaviour of the sensor is similar to that of common inertial sensors when it is subjected to translational excitations, but its sensitivity is completely lost at one particular frequency when it is subject to rotational excitations because of the gravity coupling.

In the second part, a SDOF seismic isolation system has been presented. It consists of a rigid frame rotating on a knife hinge, whose motion is measured using the interferometric inertial sensor. The system has been analysed and a model has been derived, which has been further used to design a controller, capable to reduce the ASD of frame vibration in a wide frequency range, extending from 0.1 Hz to 10 Hz, by a factor up to 1000. The performance has been cross-examined using a reference sensor, closely placed next to the in-loop sensor. The on-site noise floor of the INIS is derived by performing a huddle test between the in-loop sensor and the reference sensor. The experimental results have demonstrated that the closed loop performance of an active isolation system can't be solely evaluated by the performance index shown by the error sensor where a reference sensor or its noise floor is needed for fact-checking. This is because the control effort might be used to force the isolation platform to follow the noise of the error sensor instead of eliminating the platform motion. Currently the performance is limited by the sensor noise below 0.1 Hz. Improving the resolution of the inertial sensor in this frequency range is left for a future work.

CRediT authorship contribution statement

G. Zhao: Conceptualization, Methodology, Software, Investigation, Validation, Writing - original draft. **B. Ding:** Data curation, Investigation, Writing - review & editing. **J. Watchi:** Resources, Writing - review & editing. **A. Deraemaeker:** Supervision, Writing - review & editing. **C. Collette:** Funding acquisition, Conceptualization, Supervision, Writing - review & editing.

Declaration of Competing Interest

The authors declare that they have no known competing financial interests or personal relationships that could have appeared to influence the work reported in this paper.

Acknowledgments

The authors gratefully acknowledge the CSC for funding Binlei Ding (grant number: 201607650017), the French Community as part of the financing of a FRIA grant for Jennifer Watchi (grant number: FC 27289) and the FRS-FNRS for funding this research (grant agreement: F.4536.17). The authors would like also to thank Dr. Thomas Forbriger from the Karlsruhe Institute of Technology and Dr. Michel Van Camp from the Royal Observatory of Belgium. They kindly lend the STS-1V seismometers for the experiments. The authors are also grateful to the members of the LIGO Seismic Working Group for their comments and inspiring discussions. This document was assigned LIGO Document number LIGO-P1900054.

References

[1] J.T. Nelson, Recent developments in ground-borne noise and vibration control, J. Sound Vib. 193 (1996) 367–376.
[2] J.P. Talbot, H.E.M. Hunt, Isolation of buildings from rail-tunnel vibration: a review, Build. Acoust. 10 (2004) 177–192.
[3] J. Yang, S. Sun, T. Tian, W. Li, H. Du, G. Alici, M. Nakano, Development of a novel multi-layer MRE isolator for suppression of building vibrations under seismic events, Mech. Syst. Signal Process. 70–71 (2016) 811–820.
[4] B. De Marneffe, M. Avraam, A. Deraemaeker, M. Horodinca, A. Preumont, Vibration isolation of precision payloads: a six-axis electromagnetic relaxation isolator, J. Guid. Control. Dyn. 32 (2009) 395–401.
[5] F. Kerber, S. Hurlebaus, B.M. Beadle, U. Stöbener, Control concepts for an active vibration isolation system, Mech. Syst. Signal Process. 21 (2007) 3042–3059.
[6] Z.D. Xu, X.H. Huang, F.H. Xu, J. Yuan, Parameters optimization of vibration isolation and mitigation system for precision platforms using non-dominated sorting genetic algorithm, Mech. Syst. Signal Process. 128 (2019) 191–201.
[7] M.H. Kim, H.Y. Kim, H.C. Kim, D. Ahn, D.G. Gweon, Design and Control of a 6-DOF active vibration isolation system using a halbach magnet array, IEEE/ASME Trans. Mechatron. 21 (2016) 2185–2196.
[8] D. Qu, X. Liu, G. Liu, Y. Bai, T. He, Analysis of vibration isolation performance of parallel air spring system for precision equipment transportation, Meas. Control. 52 (2019) 291–302.
[9] N.Y.P. Vo, T.D. Le, Adaptive pneumatic vibration isolation platform, Mech. Syst. Signal Process. 133 (2019) 106258.
[10] J. Giaime, P. Saha, D. Shoemaker, L. Sievers, A passive vibration isolation stack for LIGO: Design, modeling, and testing, Rev. Sci. Instrum. 67 (1996) 208–214.
[11] C.M. Lee, V.N. Goverdovskiy, A.I. Temnikov, Design of springs with “negative” stiffness to improve vehicle driver vibration isolation, J. Sound Vib. 302 (2007) 865–874.
[12] G. Dong, X. Zhang, S. Xie, B. Yan, Y. Luo, Simulated and experimental studies on a high-static-low-dynamic stiffness isolator using magnetic negative stiffness spring, Mech. Syst. Signal Process. 86 (2017) 188–203.
[13] H. Pu, S. Yuan, Y. Peng, K. Meng, J. Zhao, R. Xie, Multi-layer electromagnetic spring with tunable negative stiffness for semi-active vibration isolation, Mech. Syst. Signal Process. 121 (2019) 942–960.
[14] Q. Wang, J. Zhou, D. Xu, H. Ouyang, Design and experimental investigation of ultra-low frequency vibration isolation during neonatal transport, Mech. Syst. Signal Process. 139 (2020) 106633.
[15] C. Collette, K. Artoos, A. Kuzmin, S. Janssens, M. Sylte, M. Guinchard, C. Hauviller, Active quadrupole stabilization for future linear particle colliders, Nucl. Instruments Methods Phys. Res. Sect. A Accel. Spectrometers, Detect. Assoc. Equip. 621 (2010) 71–78.
[16] F. Matichard, B. Lantz, K. Mason, R. Mittleman, B. Abbott, S. Abbott, E. Allwine, S. Barnum, J. Birch, S. Biscans, D. Clark, D. Coyne, D. DeBra, R. DeRosa, S. Foley, P. Fritschel, J.A. Giaime, C. Gray, G. Grabeel, J. Hanson, M. Hillard, J. Kissel, C. Kucharczyk, A. Le Roux, V. Lhuillier, M. Macinnis, B. O'Reilly, D. Ottaway, H. Paris, M. Puma, H. Radkins, C. Ramet, M. Robinson, L. Ruet, P. Sareen, D. Shoemaker, A. Stein, J. Thomas, M. Vargas, J. Warner, Advanced LIGO two-stage twelve-axis vibration isolation and positioning platform. Part 1: Design and production overview, Precis. Eng. 40 (2015) 273–286.
[17] F. Matichard, B. Lantz, K. Mason, R. Mittleman, B. Abbott, S. Abbott, E. Allwine, S. Barnum, J. Birch, S. Biscans, D. Clark, D. Coyne, D. Debra, R. Derosa, S. Foley, P. Fritschel, J.A. Giaime, C. Gray, G. Grabeel, J. Hanson, M. Hillard, J. Kissel, C. Kucharczyk, A. Le Roux, V. Lhuillier, M. MacInnis, B. O'Reilly, D. Ottaway, H. Paris, M. Puma, H. Radkins, C. Ramet, M. Robinson, L. Ruet, P. Sareen, D. Shoemaker, A. Stein, J. Thomas, M. Vargas, J. Warner, Advanced LIGO two-stage twelve-axis vibration isolation and positioning platform. Part 2: Experimental investigation and tests results, Precis. Eng. 40 (2015) 287–297.
[18] M. Schmidt, A. Senger, M. Hauth, C. Freier, V. Schkolnik, A. Peters, A mobile high-precision absolute gravimeter based on atom interferometry, Gyroscopy Navig. 2 (2011) 170–177.
[19] M.K. Zhou, X. Xiong, L. Le Chen, J.F. Cui, X.C. Duan, Z.K. Hu, Note: a three-dimension active vibration isolator for precision atom gravimeters, Rev. Sci. Instrum. 86 (2015) 1–4.
[20] P.G. Nelson, An active vibration isolation system for inertial reference and precision measurement, Rev. Sci. Instrum. 62 (1991) 2069–2075.
[21] F. Matichard, B. Abbott, R. Mittleman, B. Lantz, M. Mcinnis, A. Leroux, M. Hillard, S. Barnum, A. Stein, J. Kissel, C. Ramet, H. Radkins, S. Foley, S. Bisans, V. Lhuillier, Dynamics Enhancements of Advanced LIGO Multi-Stage Active Vibration Isolators and Related Control Performance Improvement, in: Proc. ASME 2012 Int. Des. Eng. Tech. Conf. Comput. Inf. Eng. Conf., Chicago, 2012, pp. 1269–1278.
[22] B. Lantz, R. Schofield, B. O'Reilly, D.E. Clark, D. DeBra, Requirements for a ground rotation sensor to improve advanced LIGO, Bull. Seismol. Soc. Am. 99 (2009) 980–989.
[23] C. Collette, S. Janssens, P. Fernandez-Carmona, K. Artoos, M. Guinchard, C. Hauviller, A. Preumont, Review: Inertial sensors for low-frequency seismic vibration measurement, Bull. Seismol. Soc. Am. 102 (2012) 1289–1300.
[24] S. Rowan, J. Hough, D.R.M. Crooks, Thermal noise and material issues for gravitational wave detectors, Phys. Lett. Sect. A Gen. At. Solid State Phys. 347 (2005) 25–32.
[25] G.W. Van Der Poel, An Exploration of Active Hard Mount Vibration Isolation for Precision Equipment, University of Twente, 2010.

[26] W. Hanka, Which parameters influence the very long period performance of a seismological station? Examples from, GEOFON Netw. (2015).
[27] E. Wielandt, G. Streckeisen, The leaf-spring seismometer: Design and performance, Bull. Seismol. Soc. Am. 72 (1982) 2349–2367.
[28] J. Watchi, S. Cooper, B. Ding, C.M. Mow-Lowry, C. Collette, Contributed review: a review of compact interferometers, Rev. Sci. Instrum. 89 (2018) 121501.
[29] F. Acernese, G. Giordano, R. Romano, R. De Rosa, F. Barone, Tunable mechanical monolithic sensor with interferometric readout for low frequency seismic noise measurement, Nucl. Instruments Methods Phys. Res. Sect. A Accel. Spectrometers, Detect. Assoc. Equip. 617 (2010) 457–458.
[30] J. Otero, Development and Characterization of an Observatory-class, Broadband, Non-Fedback, Leaf-Spring Interferometric Seismometer, University of California, 2009.
[31] M. Zumberge, J. Berger, J. Otero, E. Wielandt, An optical seismometer without force feedback, Bull. Seismol. Soc. Am. 100 (2010) 598–605.
[32] F. Acernese, G. Giordano, R. Romano, R. De Rosa, F. Barone, Mechanical monolithic horizontal sensor for low frequency seismic noise measurement, Rev. Sci. Instrum. 79 (2008).
[33] K. Venkateswara, C.A. Hagedorn, J.H. Gundlach, J. Kissel, J. Warner, H. Radkins, T. Shaffer, B. Lantz, R. Mittleman, F. Matichard, R. Schofield, Subtracting tilt from a horizontal seismometer using a ground-rotation sensor, Bull. Seismol. Soc. Am. 107 (2017) 709–717.
[34] B. Ding, G. Zhao, J. Watchi, C. Collette, Huddle test of optical inertial sensors combined with slightly damped mechanics, in: Int. Conf. Noise Vib. Eng., Leuven, Belgium, 2018, pp. 1471–1479.
[35] W. Yin, Y. Wei, T. Liu, Y. Wang, A novel orthogonalized fractional order filtered-x normalized least mean squares algorithm for feedforward vibration rejection, Mech. Syst. Signal Process. 119 (2019) 138–154.